

This item was submitted to [Loughborough's Research Repository](#) by the author.
Items in Figshare are protected by copyright, with all rights reserved, unless otherwise indicated.

Physico-chemical and dielectric parameters for the monitoring of carbon sequestration in basalt and silica media

PLEASE CITE THE PUBLISHED VERSION

<https://doi.org/10.1016/j.eti.2020.101052>

PUBLISHER

Elsevier

VERSION

AM (Accepted Manuscript)

PUBLISHER STATEMENT

This paper was accepted for publication in the journal Environmental Technology & Innovation and the definitive published version is available at <https://doi.org/10.1016/j.eti.2020.101052>.

LICENCE

CC BY-NC-ND 4.0

REPOSITORY RECORD

Rabiu, KO, LK Abidoye, and Diganta Das. 2020. "Physico-chemical and Dielectric Parameters for the Monitoring of Carbon Sequestration in Basalt and Silica Media". Loughborough University.
<https://hdl.handle.net/2134/12652499.v1>.

PHYSICO-CHEMICAL AND DIELECTRIC PARAMETERS FOR THE MONITORING OF CARBON SEQUESTRATION IN BASALT AND SILICA MEDIA

K. O. Rabi^{1,2}, L. K. Abidoye^{1,2}, and D. B. Das^{1,*}

¹Chemical Engineering Department, Loughborough University, Loughborough, Leicestershire, LE11 3TU United Kingdom

²Current address: Civil Engineering Department, Osun State University, Osogbo, Nigeria

*Corresponding Author (E-mail: d.b.das@lboro.ac.uk)

Abstract

Currently, there are concerns about the safety of carbon sequestration in the geological media. To assuage this concern, scientists and engineers have the tasks to demonstrate fool-proof and comprehensive techniques that can monitor the movement, or otherwise, concentration of the injected CO₂ in the subsurface. In this work, well-defined laboratory experiments were used to demonstrate the key physico-chemical characteristics and dielectric parameters that are useful in monitoring carbon sequestration sites. The porous materials used were basalt and silica sand samples to demonstrate the possibility of CO₂ injection into different media. To simulate the resident fluids, distilled and brine water samples were used in separate experimentations. Also, the pressures and temperatures were chosen to correspond to different geological depths which are relevant for CO₂ injection. The pH, bulk electrical conductivity (σ_b) and bulk dielectric permittivity (ϵ_b) of the system were measured for the two different media. On one hand, the decrease in pH was clearly observed in both the basalt and silica sand after the exposure to CO₂. On the other hand, σ_b and ϵ_b increased as CO₂ was injected. Our results further revealed a higher ion mobilization potential in basalt medium than that in silica sand. This results in lower pH and higher electrical conductivity in the basalt medium than the silica medium. Thus, a simultaneous measurement of pH, σ_b and ϵ_b are proposed as a multiparameter approach to monitor CO₂ leakage from the storage reservoir. As far as we are aware, this is the first work in the open literature that reports simultaneous dielectric and electrical behaviours of CO₂-water-porous media system for basalt porous medium in connection with carbon sequestration.

Keywords: Basalt; silica; shallow aquifer; distilled water; brine; pH; bulk electrical conductivity (σ_b); bulk dielectric permittivity (ϵ_b)

1 Introduction

Carbon capture and sequestration (CCS) is a promising approach for reducing atmospheric CO₂ emission (Abidoye and Das, 2020; Kim et al., 2018; Terzi et al., 2014). The process starts with the capture of CO₂ primarily from power plants, transport through pipeline or ships and injection into a geological formation (Rabi¹ et al., 2017b; Myer, 2011). Subsurface formations such as depleted hydrocarbon fields (Adebayo et al., 2017; Cao et al., 2020), saline aquifers (Borner and Spitzer, 2019), basalts (Snaebjornsdottir et al., 2020) and un-mineable coal seams (Talapatra, 2020) have been identified to be suitable as CO₂ repositories (Metz et al., 2005; Cao et al., 2020). In particular, saline aquifers have been suggested to provide an enormous potential of CO₂ storage capacity when compared with the other geological formations (Metz et al., 2005; Snaebjornsdottir et al., 2020). On the other hand, depleted oil and gas reservoirs can provide both economic and CO₂ storage advantages. Basalt repositories are now gaining popularity as the site for CO₂ sequestration because they have the potential to store CO₂ permanently without any risk of leakages after storage.

The major trapping mechanisms that take place during CO₂ sequestration in saline aquifers are structural, residual, solubility and mineral trapping (Rabi¹ et al., 2017a; Metz et al., 2015). Previous studies have shown that salinity has a significant influence on CO₂ trapping mechanisms (Al-Khdeewi et al., 2017; Kumar et al., 2020). For example, lower salinity enhances residual and solubility trapping significantly and prevents the free mobility of CO₂ in the aquifer. Salinity is less

important in basalt rock but, its consideration is essential in saline aquifers typically composed of silica sand. Injection of CO₂ into saline aquifer has been considered as a two-phase flow process because the injected CO₂ (non-wetting phase) displaces the resident brine water (wetting phase) during the drainage process (Abidoye and Das, 2020; Ajayi et al., 2019; Cao et al., 2020). On the other hand, when the injection of CO₂ stops, the resident brine water (wetting phase) tends to displace the CO₂ (non-wetting phase) during an imbibition process (Ajayi et al., 2019; Cao et al., 2020). These flow processes are expected to occur in presence of some geochemical reactions, for instance, reactions between water, CO₂ and silica/basalt minerals can lower the pH (Little and Jackson, 2010). The reactions can buffer the fluid pH and increase alkalinity (Snaebjornsdottir et al., 2020; Kampman et al., 2014) which have a direct effect on dielectric properties of the media. The effect of rock-fluid reactions/interactions on CO₂ solubility which affect the storage capacity of CO₂ sequestration in saline aquifers have been studied by Emami-Meybodi et al. (2015) and Erfani et al. (2020). Emami-Meybodi et al. (2015) have reported a feasibility for enhancing CO₂ dissolution by using a method that relies on injecting water on top of CO₂ plume. Due to the geochemical reactions of CO₂ and brine with the resident minerals, the pH and ion concentration of the brine change in the reservoir, and hence, the dielectric properties of the reservoir. Erfani et al. (2020) have studied the spatial and temporal dependency of such geochemical effects during CO₂ sequestration in geological formations.

Generally, CO₂ is injected as a supercritical fluid (i.e., pressure above 73 bar and temperature above 31.1°C) and at the depth of 800m or below (Rabiu et al., 2017a; Abidoye et al., 2014; Holloway, 2007; Metz et al., 2005). Supercritical CO₂ is denser than gaseous CO₂ but has lower density than the brine in the porous media (Rabiu et al., 2017a; Metz et al., 2005; Abidoye et al., 2014). Thus, after a CO₂ injection cycle stops, the supercritical CO₂ tends to move up to the confining layer due to the buoyancy force, i.e., the difference in densities between the injected CO₂ and the resident brine (Altman et al., 2014; Ajayi et al., 2019; Khudaida and Das, 2014; Suekane et al., 2008; Cao et al., 2020). It is therefore important to ensure that the caprock in any CCS site is fully characterised to determine if there is any fault or fracture that might make the CO₂ storage ineffective. Appropriate pH sensors can be used as an indicator to detect the leakage of CO₂ (Blackford et al., 2020).

While the CCS is a feasible option to mitigate the problem of CO₂ emission, the interplays of different parameters during CO₂ injection are still not fully understood. This is because a number of parameters such as CO₂ injection pressure, temperature and brine salinity govern the behaviour of CO₂ spread and mixing in the subsurface. Also, some studies argue that an increase in the reservoir pressure during the CO₂ injection will trigger earthquakes and consequently create faults or micro-fractures within the geological formation, which can eventually lead to CO₂ leakage (Szulczewski, 2013; Rabiu et al., 2017a). The faulty caprock will allow the leakage of CO₂ through the surface and subsurface where the potable drinking water is overlaid. This can result in the groundwater being contaminated and becoming more acidic, and therefore threatening the ecological system (Gupta and Yadav, 2020). Therefore, accurate monitoring of CO₂ concentration during and after a CCS project is paramount for an efficient and effective CCS project.

Seismic methods have been used for monitoring of CO₂ in the subsurface, but they are costly, and can usually quantify a limited range of CO₂ saturations accurately (Ajayi et al., 2019; Furre et al., 2017). Electrical and electromagnetic methods, e.g., electrical resistivity tomography (ERT), electromagnetic resistivity (ER), geoelectrical method (GM), electromagnetic induction tomography (EMIT), are other important approaches that may be used for the quantification of CO₂ saturation (Dafflon et al., 2012; Rabiu et al., 2017b; Ajayi et al., 2019). Wan et al. (2018) earlier examined the feasibility of permanent gravity gradiometry monitoring of geological CO₂ storage using a method involving both surface and borehole measurements. Yang et al (2019) evaluated four surface-based geophysical methods for monitoring brine and CO₂ leakage in sources of underground drinking water overlying a CCS site, and they concluded that it was important to combine downhole measurements with geophysical methods that can monitor both CO₂ concentrations and total dissolved solids (TDS) to improve CO₂ leak detection. Song et al. (2020) reported the application of an artificial neural network (ANN) in predicting the efficiency and effectiveness of CO₂ trapping mechanisms in geological carbon sequestration and concluded that ANN model is an important tool for predicting the

effectiveness of CO₂ storage in a site. ANN model such as the one reported by Song et al (2020) is expected to be useful in the analysis of the monitoring data from existing CCS sites.

It can be assumed that the CO₂ storage site selected for any CCS process is free from any potential leakage of CO₂ after proper characterisation. However, monitoring the site is still required for the reliability of the process as well as regulatory purposes (White et al., 2020). As shown in Figure 1, potable water aquifer is situated above the sediment. The leaked CO₂ follows a pathway (fractured caprocks) to reach the potable water aquifer and consequently contaminates it. Therefore, in this study, a portable and reliable *early warning monitoring method* (EWMM) for key parameters are conceptualised to characterise the potable groundwater contaminated by CO₂. The methods and parameters were chosen in a way so as to promote straightforward techniques that would lead to the safety of geological sequestration site by engendering early warning in the case of CO₂ leakage. These methods or techniques include dielectric permittivity, electrical conductivity and pH of the CO₂-water-porous media system.

By characterising the multiphase system (CO₂-water-porous media system), the changes in values of the dielectric permittivity, electrical conductivity as well as the pH with time, temperature, pressure and brine/water system will be recorded simultaneously and continuously. The trends observed in these parameters will serve to programme an automated alarm system. In case of any CO₂ leakage, a signal will be sent to the sound alarm system and, this alerts the control/monitoring personnel to assess the situation and take appropriate measures. To further simplify the task of the measurements, time-domain reflectometry (TDR) was used to simultaneously measure the bulk dielectric permittivity and electrical conductivity of CO₂-water-porous media system. This approach confers additional assurance on the monitoring signals from sequestration system. It also eliminates any time lag between the two parameters. The other parameter, pH, was measured by stand-alone pH sensor, by taking fluid samples before and after the experiment.

A previous study (Abidoye and Das, 2015b) investigates the monitoring of CO₂ leakage using dielectric properties, pH and membrane, but their work is limited to the effects of different depths. Similarly, Lamert et al. (2012) and Kharaka et al. (2010) investigate the changes in the potable groundwater chemistry after contamination with CO₂. They conclude that the dissolution of CO₂ in the groundwater reduces the pH and become toxic, which will have negative implications on the aquatic animals. Bosch et al. (2016) and Borner et al. (2017) analyse geoelectrical properties of CO₂-brine-rock interaction to detect any possible CO₂ leakage. Also, Falcon-Suarez et al. (2017) develop a multiparameter, thermo-hydro-mechanical-chemical database required to validate monitoring tools and simulators for prediction of geo-mechanical properties of CO₂ sequestration reservoirs. However, sufficient number of studies that deal with monitoring the leakage of CO₂ in various groundwater types (e.g., distilled water, tap water, MgCl brine water and NaCl brine water) that can provide a broad understanding of the relevant issues are still lacking, particularly since different groundwater types contain various constituents of ions and minerals. Also, the porous materials used in the present study are basalt and silica sand.

In addressing the above points, well-defined laboratory experiments (static flow conditions) were used to identify the significance of the physico-chemical characteristics and dielectric parameters that are useful in monitoring carbon sequestration sites with particular reference to sites containing silica and basalt medium.

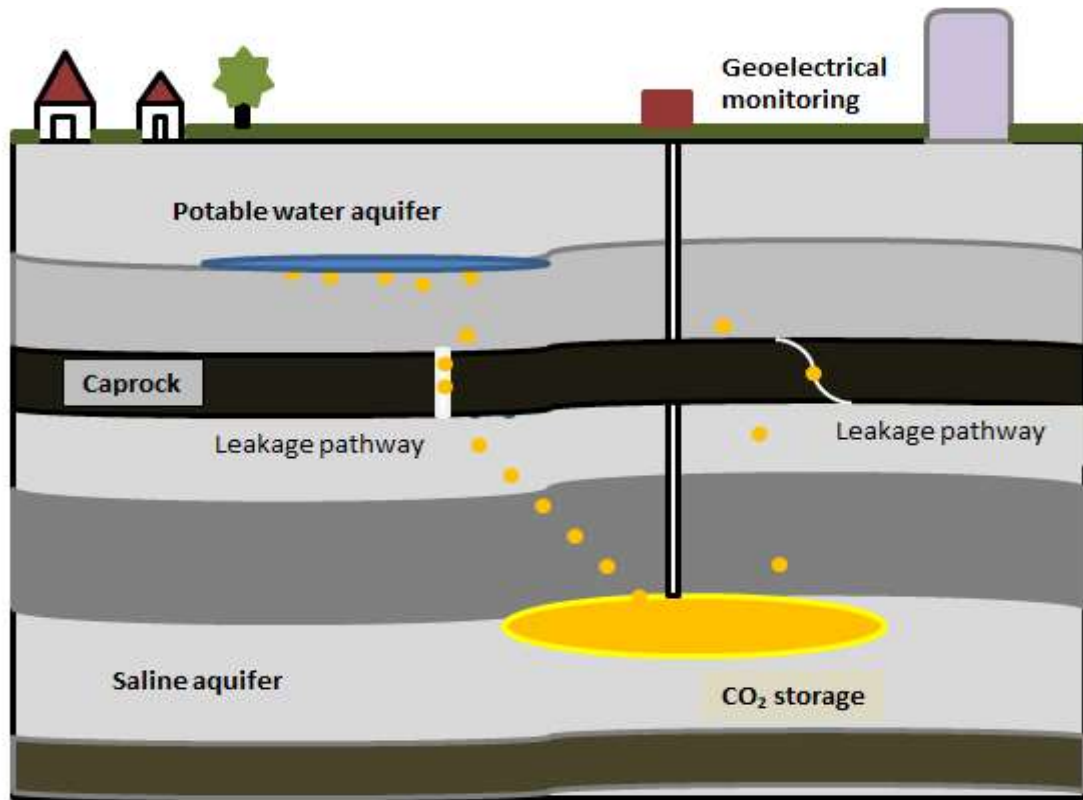


Figure 1 Schematic diagram of CO₂ leakage into potable groundwater aquifer

2 Methodology

The laboratory experiment was designed to monitor the presence of CO₂ in porous media saturated with distilled, tap and brine water. The porous materials used are silica and basalt sand and the characteristics of the samples used are described in Table 1. The time-domain reflectometry (TDR) probe was prepared in-house (Abidoye and Das 2015a; Rabiou et al., 2017b) and used to measure both bulk dielectric permittivity and bulk electrical conductivity simultaneously. In-situ measurement of the bulk electrical conductivity and bulk dielectric constant data acquired by the TDR were automatically transferred to the data acquisition system (CR10X datalogger, Campbell Scientific Ltd, Shepshed, UK). The pH measurements were done using a digital pH meter (Fisher Scientific, Loughborough, UK). The pH was calibrated before each experiment. The pH measurement of the water sample was taken before the injection of CO₂ and at the end of the experiment when the CO₂ had already dissolved in the water.

2.1 Materials and Methods

This work investigated two unconsolidated sand samples, silica sand (Minerals Marketing Company, Cheshire, UK) and basalt sand (Aqua Maniac, Delaware, USA). The physical properties such as porosity and average particle size of each mentioned porous materials were determined experimentally which are listed in Table 1. The porosity of the sand material was determined by packing porous material (Basalt/silica sand) into a cylinder of known volume and saturating the bed with a measured amount of water. The porosity was then calculated using the Equation 1.

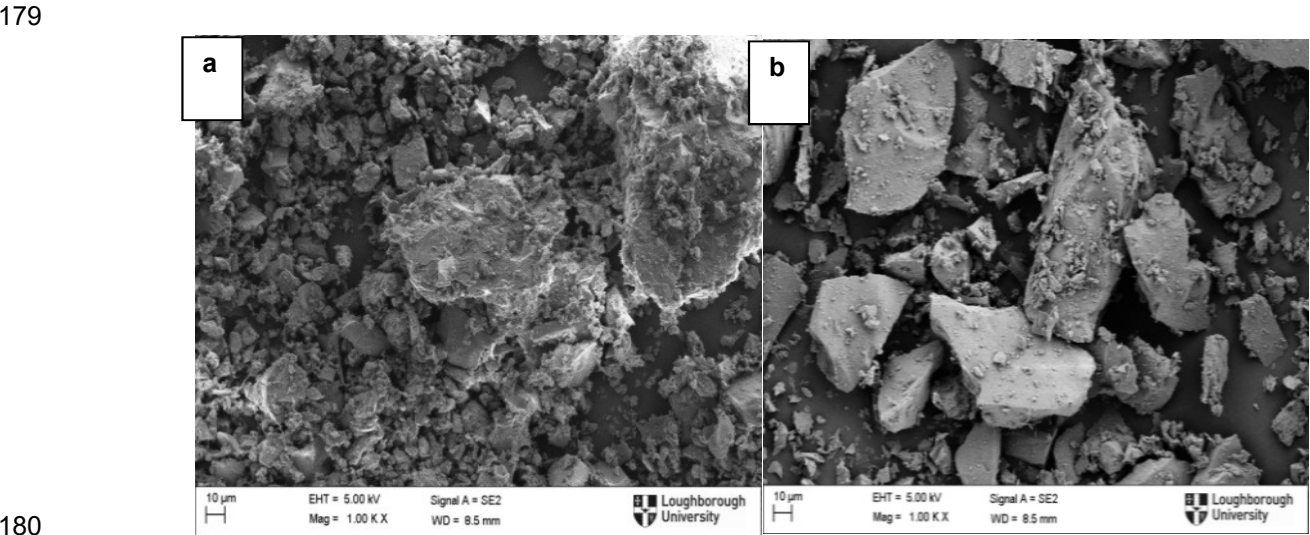
$$\phi = \frac{R_t - R_s}{R_t} = \frac{R_v}{R_t} = \frac{R_w}{R_t} \quad (1)$$

where ϕ is porosity, R_t is the total volume of a porous media sample, R_s is the volume of solids in the sample, R_v is the volume of openings (voids), and R_w is the volume of water that will occupy the voids space. Before the porosity experiment, the silica sand and basalt were washed with distilled water and dried to remove any clay content. Moreover, SEM (Zeiss 1530VP) images were taken before the experiment to examine surface morphology and roughness of the particles which make up the porous

172 materials used. As shown in Figure 2, basalt sand particles have a hexagonal shape while silica sand
173 particles are more angular.

174
175 **Table 1** Characteristics of the porous materials used in the experiments

176	Parameters	Silica Sand	Basalt Sand
177	Porosity (%)	39±0.25	42±0.30
178	Average particle size (µm)	968±253	1016±296



182 **Figure 2** Scanning electron microscope (SEM) images of: (a) basalt and (b) silica sand particles.

184 **2.2 Experimental Methods and Procedures**

185 The stainless-steel sample holder used in the experiment was fabricated in-house in the workshop at
186 Loughborough University. It had dimensions of 4 cm in height and 10 cm in diameter. The simulated
187 water used in the experiment was either distilled or brine water. The brine water was prepared in the
188 laboratory by adding sodium chloride or magnesium chloride salts to the distilled water. The sodium
189 chloride and magnesium chloride salts were purchased from Fisher Scientific, Loughborough (UK).

190 To start the experiment, 500g of the sand particles (silica or basalt) were deposited into the sample
191 holder and saturated with distilled or brine water. It was then covered by the stainless-steel top end
192 piece and all the joint bolts were firmly tightened to avoid any leakage of the CO₂ during the
193 experiment. Before CO₂ injection started, the samples of the brine and distilled water were collected
194 from saturated porous media and measured with the pH probe/meter. The pH probe/meter was
195 purchased from Fisher Scientific (Loughborough, UK). The CO₂ gas (99.9% purity) used in this work
196 was procured from BOC gases (Leicester, UK).

197 The ScCO₂ fluid pump (Teledyne Isco, Lincoln NE) was filled with CO₂ from the CO₂ cylinder by
198 opening valve 1 (V-1; Figure 3). Thereafter, V-1 was closed and the ScCO₂ fluid pump was set to the
199 experimental pressure. The heater was switched on and also set at the experimental temperature.
200 When temperature and pressure reached the predetermined values, i.e., when there was equilibrium
201 in experimental conditions (both temperature and pressure), V-3 was opened (see Figure 3) and the
202 CO₂ was injected. This work simulated static potable groundwater that is not moving or moving very
203 slowly. Therefore, the experiment was carried out in static conditions (i.e., CO₂ was accumulated or
204 dissolved in water). Some experiments were carried out for short periods of time while others were left
205 for longer periods of time. The in-situ electrical properties were measured automatically by data
206 logger, and the data were collected by personal computer (see, e.g., Figure 3). The pH probe/meter
207 measured the water sample before and after the experiments. It is very important to carry out

208 a calibration prior to making each measurement in order to assure that the reading which is given by
209 the pH meter is accurate.

210 **2.3 Design of the experimental conditions**

211 The experiments were designed so as to simulate the conditions that are encountered during the
212 leakage of CO₂ from a geological sequestration site in the shallow subsurface, i.e., temperature,
213 pressure and salinity that are relevant to potable shallow aquifers. It can be recalled that the leakage
214 of CO₂ from storage aquifers into shallow aquifers can lower the pH of the groundwater and make it to
215 become more acidic, which will have a negative impact on the aquatic animals.

216 This study developed an innovative method of monitoring the behaviour of the contaminant CO₂ in the
217 groundwater aquifers. The geological conditions were defined using the reports of the Abidoye and
218 Das (2015a) and the modified conditions were listed in Table 2.

219 On one hand, the in-situ measurements of the electrical parameters (i.e., bulk dielectric permittivity
220 (ϵ_b) and the bulk electrical conductivity (σ_b)) were measured simultaneously; and on the other hand,
221 the water samples were collected before and after the experiment for the pH measurements. Figure 3
222 shows the schematic diagram of the CO₂ leakage into the potable groundwater aquifer.

223 The soil electrical properties and water saturation determine the amount of CO₂/brine in reservoirs.
224 The electrical properties is often modelled empirically using the Archie's law (Archie, 1942); however,
225 the relation is known to be limited in its applicability as it works best when the pore water conductivity
226 does not change (Borner et al. 2013). The law is purely an empirical law and attempts to quantify ion
227 transport in clean and consolidated sand. For example, we can consider Jin and Yang (2020) who
228 have attempted a theoretical and experimental quantification of the relationship between electrical
229 resistivity and hydrate saturation in sand material. The author concluded that the ERTs are in better
230 agreement with the experimental measurements, while the Archie's law introduced a larger error at
231 higher hydrate saturation. We have used Archie's law in our past work where the experimental
232 conditions are within the range of applicability of the law (Abidoye and Das, 2015a); however, in this
233 work, the pore water conductivity is expected to change at the pore-scale, particularly in basalt media.
234 Furthermore, we use unconsolidated porous domain with a view to identify the key physico-chemical
235 and dielectric characteristics. Considering the above points, this work does not attempt to use
236 Archie's law to fit the data obtained in this work.

237 **2.4 pH Measurement**

239 The pH of the solution was measured using the Hydrus 500 pH meter (Fisher Scientific,
240 Loughborough, UK). The water sample was collected before and after the experiment for the pH
241 measurement. The pH meter was calibrated after each experiment to ensure consistent results.

242 **2.5 Time-domain reflectometry (TDR)**

244 The TDR probes used in this work were fabricated in the workshop (Loughborough University, UK)
245 (Abidoye and Das 2015a; Rabiou et al., 2017b). The electrical pulses were generated by the TDR100.
246 These pulses travelled through the coaxial cables that were connected to the TDR probes. The
247 working procedure of the TDR probe can be found in the work of Rabiou et al. (2017b). The TDR
248 measures both the bulk dielectric permittivity and bulk electrical conductivity simultaneously.

249 Recently, Rabiou et al. (2017b) and Abidoye and Das (2015a) carried out investigations on the effects
250 of flow experiments on the electrical properties and water saturation relationships using locally-
251 fabricated TDR. Some parameters such as pressure, temperature and salinity were shown to
252 influence the dielectric and water saturation relationships during the flow experiments. On the other
253 hand, pH, flow rate and salt types were concluded to show no significant effect (Rabiou et al., 2017b;
254 Abidoye and Das, 2015a). The current work investigates the dielectric and physico-chemical
255 monitoring of the dissolution of CO₂ in water (i.e., brine, distilled, tap) during a static experiment.

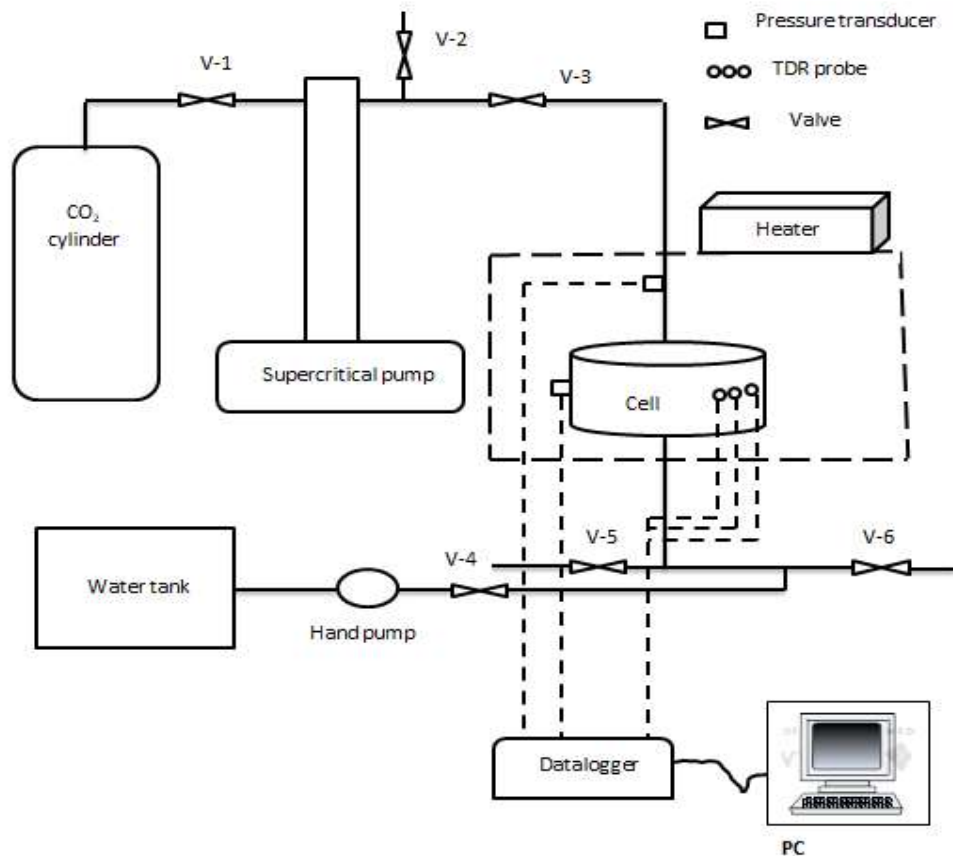


Figure 3 A schematic diagram of the static experimental system (adapted from Rabiou et al., 2017b).

Table 2 List of experimental conditions simulated in this work (the geothermal gradients were determined using the reports of Abidoye and Das (2015b))

Exp.	Porous Media	Simulated Aquifer groundwater	Depth (m)	Temperature (°C)	Pressure (bar)	Injection duration (min)	CO ₂ Phase
1	Basalt sand	Distilled water	200	31	54	30	Gas
2	Silica sand	Distilled water	200	31	54	30	Gas
3	Basalt sand	Brine water	200	31	54	30	Gas
4	Silica sand	Brine water	200	31	54	30	Gas
5	Silica sand	Distilled water	100	25	27	360	Gas
6	Silica sand	Tap water	100	25	27	360	Gas
7	-	Tap water	100	25	27	360	Gas
8	-	Distilled water	100	25	27	360	Gas

http://www.peacesoftware.de/einigewerte/co2_e.html

263 3 Results and Discussion

264 3.1 pH Analysis

265 The chemical composition of the experimental potable groundwater conducted in this study was
 266 significantly affected by CO₂ exposure. The results of the pH analyses before and after the
 267 experiments are reported in Table 3. As the table shows, there is a significant pH drop in the distilled
 268 water + basalt + CO₂-reacted solution (i.e. from 8.41±0.09 to 6.47±0.12) after short-term CO₂
 269 injection. However, there is a lesser degree of fall in the pH for the distilled water + silica sand + CO₂-
 270 reacted solution (i.e., from 6.12±0.07 to 5.65±0.10). The observed reduction in the pH values can be
 271 attributed to the dissolution of injected CO₂ in distilled water which resulted in an acidic medium, i.e.,
 272 formation of carbonic acid in the porous medium as shown in equation (2).



275
 276 As expected, this pH reduction in the CO₂-H₂O-sand systems confirms the reactive nature of the
 277 injected CO₂ (Terzi et al., 2014; Rabiou et al., 2017a). There was more significant drop in pH when
 278 CO₂ reacted with water in the basalt sand medium than in water-silica sand medium. This can be
 279 attributed to the presence of some minerals such as magnesium, iron and aluminium in the basalt
 280 sand (Metz et al., 2005; Petrik and Mabee, 2005). The quantities of these minerals are lower in silica
 281 sand (see Figures A1, A2 at the appendix). Studies have shown that basalt rocks are suitable for
 282 permanent sequestration of CO₂ but their conversion into solid carbonates are very slow (Rabiou et al.,
 283 2017a,b; Saebjornsdottir et al., 2020). In order to minimise the leakage of CO₂ into potable
 284 groundwater, basalt medium offers more promise than silica sand medium.

285 **Table 3** Changes in pH of water-saturated basalt and silica porous media before and after CO₂
 286 injection for short experiment (30 minutes)

<i>Simulated Potable Aquifer</i>	<i>Depth (m)</i>	<i>pH before CO₂ injection in the saturated silica sand</i>	<i>pH after CO₂ injection in the saturated silica sand</i>	<i>pH before CO₂ injection in the saturated basalt sand</i>	<i>pH after CO₂ injection in the saturated basalt sand</i>
<i>Distilled water</i>	200	6.12±0.07	5.65±0.10	8.41±0.09	6.47±0.12
<i>Brine water</i>	200	5.79±0.10	5.55±0.09	7.40±0.08	5.97±0.10

287

288 3.2 Electrical Conductivity and Dielectric Permittivity

289 One of the environmental issues of the CO₂ sequestration process is the potential leakage of the CO₂
 290 from the storage reservoirs into the fresh groundwater aquifers. This consequently contaminates the
 291 potable water and makes it a threat to aquatic animals and living organisms. The characteristics of the
 292 water-saturated porous material when contaminated by CO₂ are expected to be different for various
 293 types of aquifers. For example, the characteristics in CO₂-H₂O-basalt sand will be different from CO₂-
 294 H₂O-silica sand. This can be attributed to the presence of different mineral constituents in various
 295 water samples. Work on the static experiment on the monitoring of dielectric properties of CO₂-water-
 296 limestone/silica sand has been studied for different geological depths (Abidoye and Das, 2015a) and
 297 the authors have concluded that different depths have different effects on the dielectric properties.

298 In the present study, the results of the investigation of the scenarios in which the dielectric
 299 characterisation was used to monitor the potable groundwater contaminated by leaked CO₂ are
 300 presented. The effect of different types of potable groundwater on the dielectric properties was
 301 examined. This work simulated four distinct fluids in analogy to the common mixtures of fluids or
 302 solutions found in groundwater aquifers (for example, see Table 4).

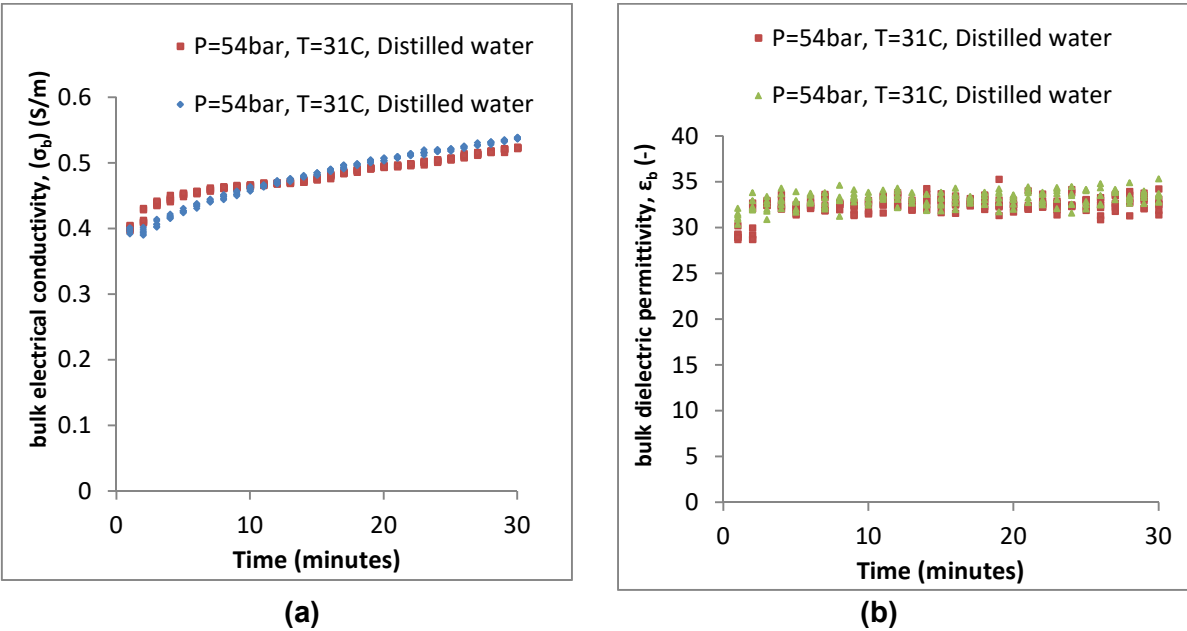


Figure 4 (a) Repeatability of σ_b - t and (b) ϵ_b - t relationships of silica sand saturated by distilled water.

Figure 4 (a,b) shows the repeatability of σ_b - t and ϵ_b - t relationships. The bulk electrical conductivity slightly increased when exposed to CO_2 , a phenomenon that arises from the dissolution of CO_2 in water, as has been well documented in the literature (see, e.g., Abidoye and Das, 2015b; Dethlefsen et al., 2013; Lamert et al., 2012). The increase in the bulk electrical conductivity can be attributed to the increase in the ions, which is caused by the dissolution of CO_2 in water. From the reaction engineering point of view, the dissolution behaviour of the CO_2 in water results in more acidic fluid conditions in the silica sand- CO_2 -water system (Equation 2). On the other hand, there is no significant increase in bulk dielectric permittivity in the silica sand- CO_2 -water system when exposed to CO_2 .

As depicted in Figure 5a, there is a significant difference in the measurements of σ_b in the silica sand saturated with distilled water and silica sand saturated with 1% w/w NaCl brine, both before and after the experiment. A similar trend was observed in the basalt sand saturated with distilled water and brine water as shown in Figure 5b. The significant difference in bulk electrical conductivity between the porous media saturated with the distilled water and the porous media saturated with the brine water can be connected to the increase in the ions due to an increase in salinity in brine water (Rabiu et al., 2017b; Abidoye and Das, 2015a). The higher trend in the basalt sand can be connected to the presence of high contents of some minerals such as magnesium, iron, and aluminium in the basalt sand, which are very little in silica sand (see Figure A1, A2 in the Appendix).

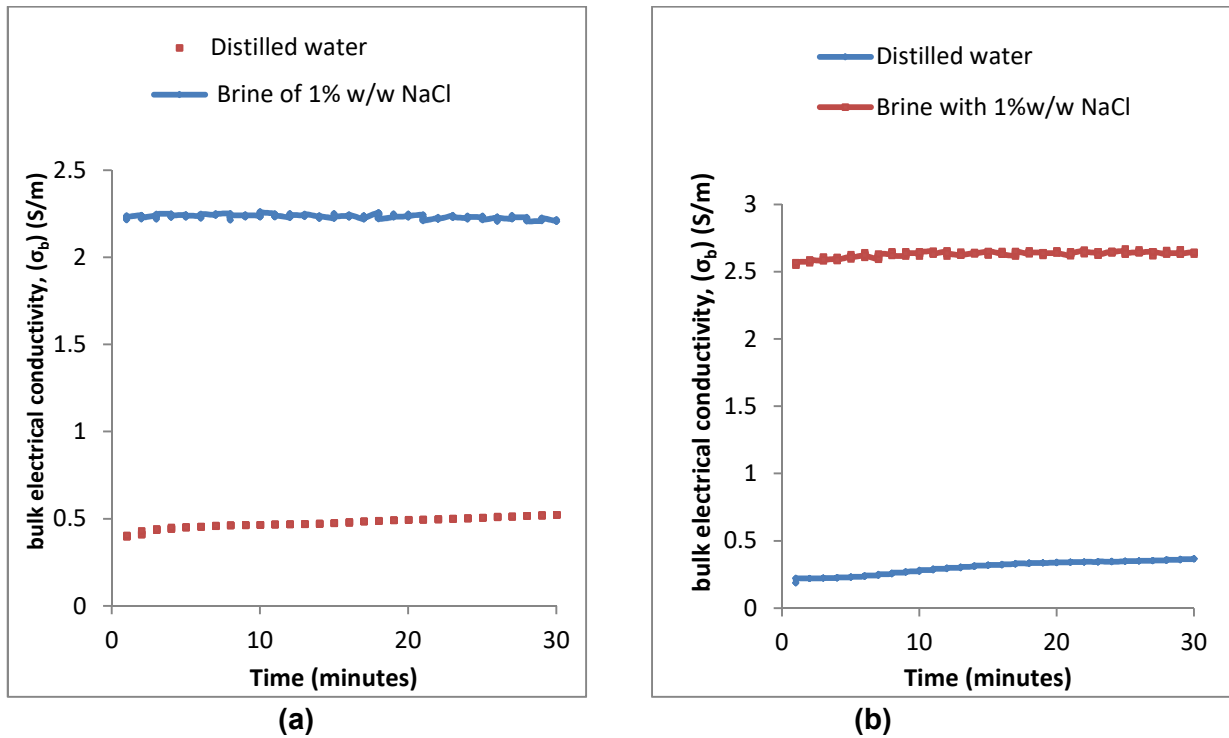


Figure 5 (a) σ_b - t relationship in silica sand saturated by distilled water and brine water of 1%w/w NaCl (b) σ_b - t relationship in basalt sand saturated by distilled water and brine water of 1%w/w NaCl.

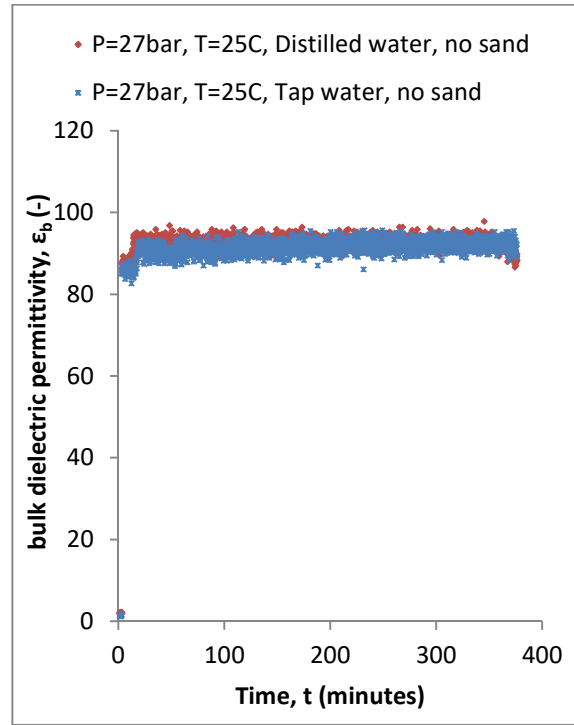
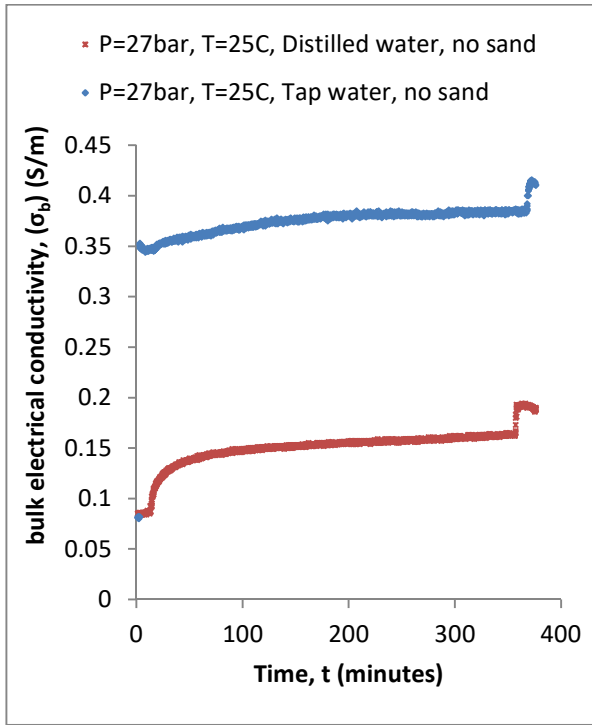
Figure 6 (a,b) represents baseline for σ_b and ϵ_b of CO_2 - H_2O without any porous media. As shown in Figure 6(a,b), there was a wide gap between (σ_b - t , ϵ_b - t) relationships of CO_2 injected into distilled/tap water and (σ_b - t , ϵ_b - t) relationships of CO_2 injected into silica sand saturated with distilled/tap/brine (Figure 7a,b), and this can be attributed to the presence of porous media.

Moreover, this study focuses on understanding the potential impacts of water quality on the sand/water/ CO_2 system, chosen on the basis of different qualities of groundwater reported in the literature (Table 4). CO_2 injection into three different potable groundwater types with the same pressure and temperature conditions in the laboratory scale have been carried out to assess the impact of groundwater types on the dielectric properties during the monitoring process in silica/basalt sand-water- CO_2 systems.

The bulk electrical conductivity and bulk dielectric permittivity of the silica sand saturated by distilled, tap and brine water were measured and shown in Figure 7(a,b). For the silica sand saturated by either distilled or tap water, the baseline of the bulk electrical conductivity (σ_b) before their exposure to CO_2 measured an average value of 0.2 S/m (± 0.1 S/m standard deviation).

Table 4 Different fluids that resemble several possible groundwater aquifers

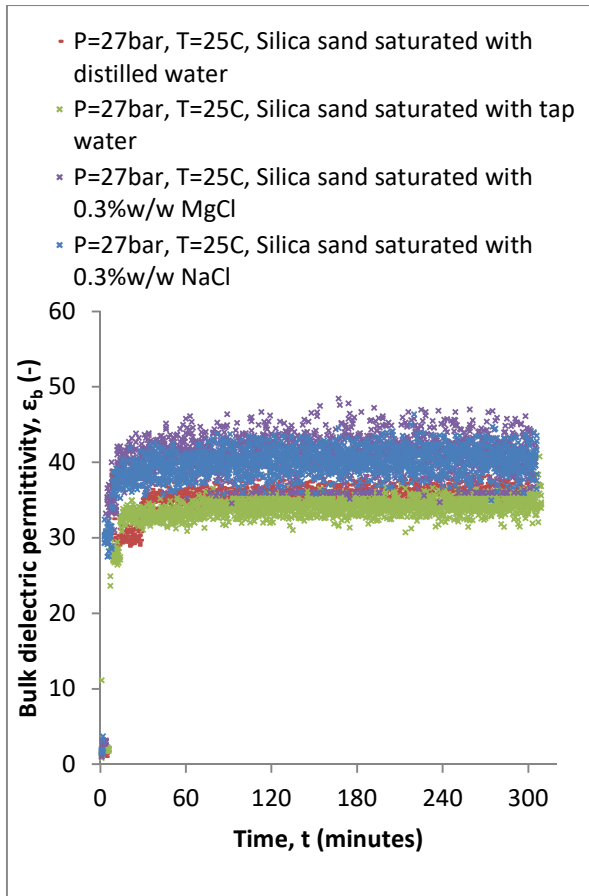
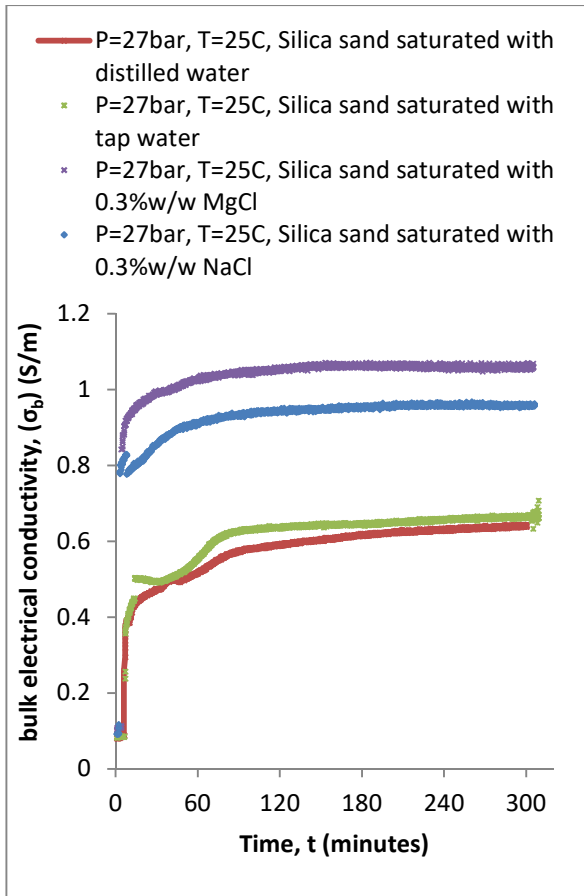
	Fluid 1	Fluid 2	Fluid 3	Fluid 4
pH	6.73	7.44	6.95	7.04
Fluid component	Distilled water	Tap water (consists of Ca^{2+} , Mg^{2+} , K^+)	Distilled water + 0.3% w/w NaCl	Distilled water + 0.3% w/w MgCl
Potable aquifer condition	Neutral aquifer (Borner et al. 2013)	Average aquifer that is not polluted (Borner et al. 2013)	Aquifer that contain moderate NaCl salt	Aquifer that contain moderate MgCl salt



(a)

(b)

Figure 6 (a) σ_b - t and (b) ϵ_b - t relationships of CO_2 injected into distilled/tap water; it represents baseline of σ_b and ϵ_b for CO_2 - H_2O system.

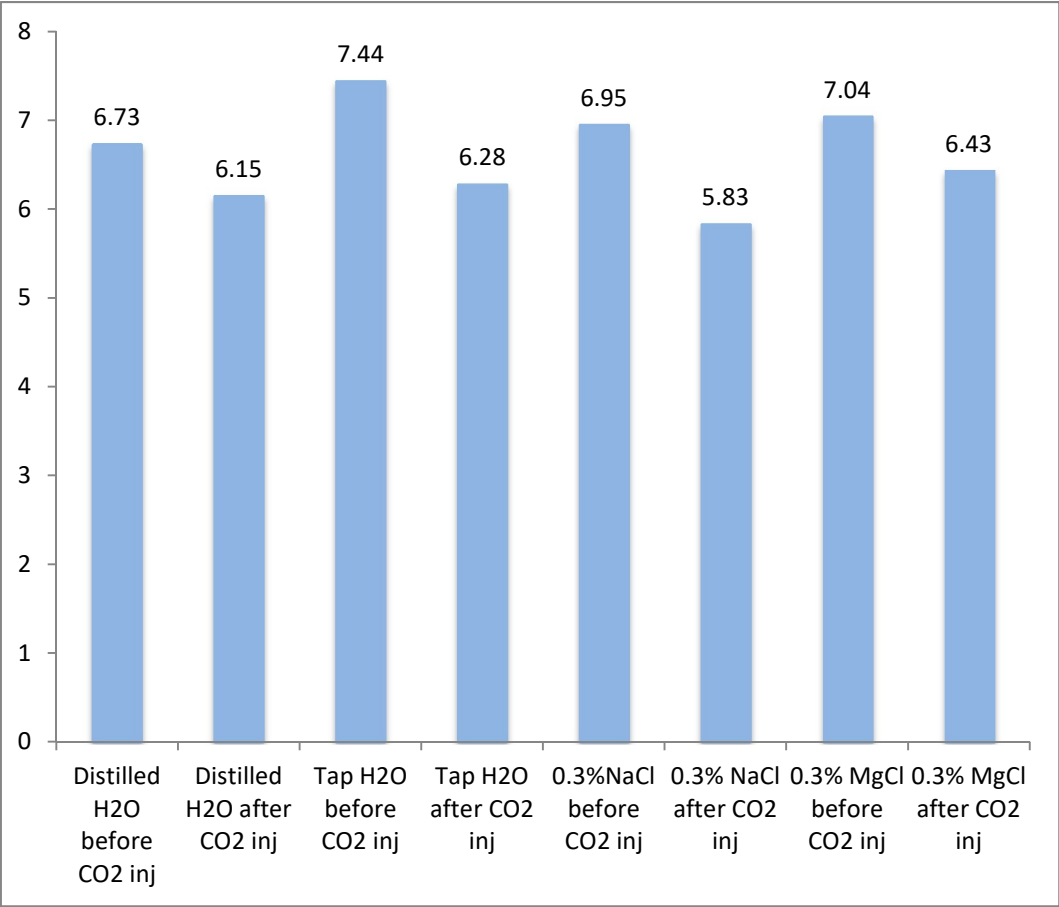


(a)

(b)

Figure 7 (a) σ_b - t and (b) ϵ_b - t relationships of CO_2 injected into silica sand saturated with distilled/tap/brine (MgCl and NaCl) water.

355 After 5 hours of CO₂ dissolution in the water, the average bulk electrical conductivity (σ_b) had
 356 increased to 0.6 ± 0.10 S/m (Figure 7a). The same trend was observed for the silica sand saturated
 357 with both MgCl and NaCl brine, i.e., their bulk electrical conductivity increased after the addition of
 358 CO₂ and this can be linked to the increase in ions due to the dissolution of CO₂ in water. This was
 359 also observed in the work of Abidoye and Das (2015b), but their work was limited to distilled water.
 360 Also, Dethlefsen et al. (2013) as well as Lamert et al. (2012) observed similar trends during the
 361 monitoring of CO₂ injection in field experiments. On the other hand, the present work uses a
 362 laboratory experiment to study the monitoring of CO₂ leakage into different types of water that can be
 363 found in groundwater aquifers. The undertaken assessment is generally representative of potable
 364 groundwater contaminated by CO₂. Also, as shown in Figure 7b, the dielectric permittivity of tap water
 365 and distilled water are very similar, i.e., both increased to 36 ± 6 after 5 hours of CO₂ dissolution in the
 366 water, but the silica sand saturated with both MgCl and NaCl brine have higher dielectric permittivity
 367 and the difference may be attributed to effect of more ions in the saline aquifers.
 368



369
 370 **Figure 8** pH of silica sand saturated with water (H₂O) before and after CO₂ injection (inj)
 371

372 In addition, Figure 8 shows that pH decreased after injection of CO₂ into distilled, tap, 0.3% w/w NaCl
 373 and 0.3% w/w MgCl brine water, respectively. Noticeably, the initial pH in the tap water has the
 374 highest in comparison with the other types of water solutions used in the experiment; and this can be
 375 attributed to the different constituents that were contained in the tap water which were absent in other
 376 water solutions. This is observed in the work of Petit et al. (2020) but their work was limited to only
 377 water, water and sand or water and limestone; and they concluded that pH measurements seem to be
 378 tremendous indicators for monitoring a gas plume during CO₂ geological storage. Furthermore, as
 379 clearly illustrated in Figure 8; the sodium chloride brine solution after exposure to CO₂ has the lowest
 380 pH. This is followed by the distilled water solution, the tap water solution and the MgCl brine solution,
 381 respectively. Hence, the highest acidity was found in the sodium chloride brine solution after CO₂
 382 exposure while the lowest acidity was observed in the magnesium chloride brine solution.

383 4 Conclusion and Further Work

384 The work presented in this paper attempts to identify the key physico-chemical and dielectric
385 characteristics of basalt and silica sites contaminated by CO₂ due to a CCS project. In addressing this
386 aim, the bulk electrical conductivity (σ_b) and bulk dielectric permittivity (ϵ_b) of basalt and silica
387 samples were measured simultaneously using the time domain reflectometry (TDR) technique while
388 the pH meter/probe was used to measure the pH of the water sample collected before and after the
389 static flow experiment. After exposure to CO₂, the decrease in pH was clearly observed in both basalt
390 and silica sand samples. The decrease in pH is was attributed to the dissolution of the CO₂ in the
391 water which changed the solution into carbonic acid. On the other hand, the bulk dielectric permittivity
392 increased as CO₂ started to be injected. Contrarily, the bulk electrical conductivity shows no changes
393 after CO₂ injection started but increased after a while. This can be attributed to the dissolution of CO₂
394 in water, since it takes some time before the dissolution occurs. Therefore, the bulk electrical
395 conductivity, bulk dielectric permittivity and pH can be used as in a multi-parameter tool to monitor the
396 CO₂ leakage into the potable groundwater. With CCS still being explored mostly in a few developed
397 countries in the world, these monitoring techniques could be of real practical use in the future. It is
398 therefore anticipated that the developed system can be developed further in future work, e.g., as
399 Internet of Things (IoT) system for continuous monitoring of CCS sites. It should also be stated that
400 more detailed experiments on the flow behaviour (e.g., dynamic flow of CO₂/water in the porous
401 samples) and the related effects on the physico-chemical and dielectric parameters of basalt and
402 silica media should be carried out in the future. Statistical analysis of the data generated using non-
403 linear regression may be carried out too to analyse the significance of the correlation among different
404 parameters. In addition, machine learning tools such as those reported by Song et al. (2020) may be
405 explored for analysis of the data generated by the monitoring tools at a site.

407 References

- 408 Abidoye, L.K., Das, D.B., 2015a. Geoelectrical characterization of carbonate and silicate porous
409 media in the presence of supercritical CO₂–water flow. *Geophysical Journal International*, 203(1),
410 pp.79–91. <https://doi.org/10.1093/gji/ggv283>.
- 411 Abidoye, L.K., Das, D.B., 2015b. pH, geoelectrical and membrane flux parameters for the monitoring
412 of water-saturated silicate and carbonate porous media contaminated by CO₂. *Chemical Engineering*
413 *Journal*, 262, pp.1208–1217. <https://doi.org/10.1016/j.cej.2014.10.036>.
- 414 Abidoye, L.K., Das, D.B., 2020. Impacts of dynamic capillary pressure effects in supercritical CO₂-
415 Water flow: Experiments and numerical simulations. *Advances in Water Resources*, 136, DOI:
416 10.1016/j.advwatres.2020.103504.
- 417 Adebayo, A.R., Kandil, M.E., Okasha, T.M., Sanni, M.L., 2017. Measurements of electrical resistivity,
418 NMR pore size and distribution, and x-ray CT-scan for performance evaluation of CO₂ injection in
419 carbonate rocks: A pilot study. *International Journal of Greenhouse Gas Control*, 63, pp. 1-11.
420 DOI: 10.1016/j.ijggc.2017.04.016.
- 421 Ajayi, T., Gomes, J.S., Bera, A., 2019. A review of CO₂ storage in geological formations emphasizing
422 modeling, monitoring and capacity estimation approaches. *Pet. Sci.* 16, 1028–1063.
423 <https://doi.org/10.1007/s12182-019-0340-8>.
- 424 Al-Khdeewi, E. A., Vialle, S., Barifcani, A., Sarmadivaleh, M., Zhang, Y. and Iglauder, S., 2017.
425 Impact of salinity on CO₂ containment security in highly heterogeneous reservoirs. *Greenhouse Gas*
426 *Sci Technol.* 8(1), pp. 93-105. doi:10.1002/ghg.1723.
- 427
- 428 Altman, S.J., Aminzadeh, B., Balhoff, M.T., Bennett, P.C., Bryant, S.L., Cardenas, M.B., Chaudhary,
429 K., Cygan, R.T., Deng, W., Dewers, T., DiCarlo, D.A., Eichhubl, P., Hesse, M.A., Huh, C., Matteo,
430 E.N., Mehmani, Y., Tenney, C.M., Yoon, H., 2014. Chemical and Hydrodynamic Mechanisms for

431 Long-Term Geological Carbon Storage. *J. Phys. Chem.*, 118 (28), pp. 15103–15113,
432 DOI: 10.1021/jp5006764.

433 Archie G., 1942. The electrical resistivity log as an aid in determining some reservoir characteristics.
434 *Transaction of the American Institute of Mining and Metallurgical Engineers*, 146, pp. 54–61.
435 https://personal.ems.psu.edu/~radovic/EME590_Archie_1942.pdf.

436 Blackford, J., Alendal, G., Avlesen, H., Brereton, A., Cazenave, P. W., Chen, B., Phelps, J.,
437 2020. Impact and detectability of hypothetical CCS offshore seep scenarios as an aid to storage
438 assurance and risk assessment. *International Journal of Greenhouse Gas Control*, 95,
439 102949. doi:10.1016/j.ijggc.2019.102949.

440 Borner, J.H., Herdegen, V., Repke, J., Spitzer, K., 2013. The impact of CO₂ on the electrical
441 properties of water bearing porous media – laboratory experiments with respect to carbon capture
442 and storage. *Geophysical Prospecting*, 61 (1), 446–460. doi: 10.1111/j.1365-2478.2012.01129.x.

443 Borner, J.H., Herdegen, V., Repke, J.U., Spitzer, K., 2017. Special induced polarization of the three-
444 phase system CO₂-brine-sand under reservoir conditions, *Geophysical Journal*
445 *International*, 208 (1), pp. 289-305. DOI: 10.1093/gji/ggw389.

446 Borner, J.H., Spitzer, K., 2019. Monitoring of CO₂ sequestration and leakage using borehole transient
447 electromagnetics and the DC resistivity method: a 3D feasibility study incorporating realistic
448 geological scenarios. *Society of Exploration Geophysicists International Exposition and 83rd Annual*
449 *Meeting, SEG 2013:Expanding Geophysical Frontiers*, pp. 4461-4465, doi: 10.1190/segam2013-
450 0566.1.

451 Bosch, D., Ledo, J., Queralt, P., Bellmund, F., Luquot, L., Gouze, P., 2016. Core-scale electrical
452 resistivity tomography (ERT) monitoring of CO₂-brine mixture in Fontainebleau sandstone. *Journal of*
453 *Applied Geophysics*, 130, pp. 23-36, DOI: 10.1016/j.jappgeo.2016.03.039.

454

455 Cao, C., Liu, H., Hou, Z., Mehmood, F., Liao, J., Feng, W., 2020. A Review of CO₂ Storage in View of
456 Safety and Cost-Effectiveness. *Energies*, 13(3), pp. 1-45. doi:10.3390/en13030600.

457 Dafflon, B., Wu, Y., Hubbard, S.S., Birkholzer, J.T., Daley, T.M., Pugh, J.D., Peterson, J.E., Trautz,
458 R.C., 2012. Monitoring CO₂ intrusion and associated geochemical transformations in a shallow
459 groundwater system using complex electrical methods. *Environmental Science and Technology*,
460 47(1), pp.314–321. [dx.doi.org/10.1021/es301260e](https://doi.org/10.1021/es301260e).

461 Dethlefsen, F., Kober, R., Schafer, D., Hagrey, S.A.A., Hornbruch, G., Ebert, M., Dahmke, A., 2013.
462 Monitoring Approaches for Detecting and Evaluating CO₂ and Formation Water Leakages into Near-
463 surface Aquifers. *Energy Procedia*, 37, pp. 4886–4893.
464 <https://doi.org/10.1016/j.egypro.2013.06.399>.

465 Emami-Meybodi, H., Hassanzadeh, H., Green, C., Ennis-King, J., 2015. Convective dissolution of
466 CO₂ in saline aquifers: Progress in modeling and experiments, *International Journal of Greenhouse*
467 *Gas Control*, 40, pp. 238–266, DOI: 10.1016/j.ijggc.2015.04.003.

468 Erfani, H., Babaei, M., Niasar, V., 2020. Signature of Geochemistry on Density-Driven CO₂ Mixing in
469 Sandstone Aquifers. *Water Resources Research*, 56 (3), DOI:10.1029/2019WR026060.

470 Falcon-Suarez, I., Marín-Moreno, H., Browning, F., Lichtschlag, A., Robert, K., North, L.J., Best, A.I.,
471 2017. Experimental assessment of pore fluid distribution and geomechanical changes in saline
472 sandstone reservoirs during and after CO₂ injection, *International Journal of Greenhouse Gas*
473 *Control*, 63, pp. 356-369. DOI: 10.1016/j.ijggc.2017.06.019.

474 Furre, A., Eiken, O., Alnes, H., Vevatne, J. N., Kaer, A. F., 2017. 20 years of monitoring CO₂-injection
475 at Sleipner, 13th International Conference on Greenhouse Gas Control Technologies, GHGT-13, 14-

476 18 November 2016, Lausanne, Switzerland, Energy Procedia, 114, pp. 3916 – 3926, doi:
477 10.1016/j.egypro.2017.03.1523.

478 Gupta, P.K., Yadav, B. (2020). Leakage of CO₂ from geological storage and its impacts on fresh soil–
479 water systems: a review. Environmental Science and Pollution Research, 27 (12), pp. 12995-13018,
480 DOI: 10.1007/s11356-020-08203-7

481 Holloway, S., 2007. Carbon dioxide capture and geological storage. Phil Trans. R. Soc. A, 365,
482 pp.1095–1107. doi:10.1098/rsta.2006.1953.

483 Jin, Y., Li, S., Yang, D., 2020. Experimental and theoretical quantification of the relationship between
484 electrical resistivity and hydrate saturation in porous media, Fuel, 269, DOI:
485 10.1016/j.fuel.2020.117378.

486

487 Kampman, N., Bickle, M., Wigley, M., Dubacq, B., 2014. Fluid flow and CO₂-fluid-mineral interactions
488 during CO₂-storage in sedimentary basins. Chemical Geology, 369, pp. 22-50, DOI:
489 10.1016/j.chemgeo.2013.11.012.

490 Kharaka, Y.K., Thordsen, J.J., Kakouros, E., Ambats, G., Herkelrath, W.N., Beers, S.R., Birkholzer,
491 J.T., Apps, J.A., Spycher, N.F., Zheng, L., Trautz, R.C., Rauch, H.W., Gullickson, K.S., 2010.
492 Changes in the chemistry of shallow groundwater related to the 2008 injection of CO₂ at the ZERT
493 field site, Bozeman, Montana. Environ Earth Sci, 60(2), pp.273–284.
494 <https://doi.org/10.1007/s12665-009-0401-1>.

495 Khudaida, K., Das, D.B., 2014. A numerical study of capillary pressure-saturation relationship for
496 supercritical carbon dioxide (CO₂) injection in deep saline aquifer. Chemical Engineering Research
497 and Design, 92(12), pp.3017–3030. <https://doi.org/10.1016/j.cherd.2014.04.020>.

498 Kim, C. Y., Han, W. S., Park, E., Jeong, J., Xu, T., 2018. CO₂ Leakage-Induced Contamination in
499 Shallow Potable Aquifer and Associated Health Risk Assessment. Geofluids, vol. 2018, pp. 1–
500 19. doi:10.1155/2018/4834601.

501 Kumar, R., Campbell, S., Sonnenthal, E., Cunningham, J., 2020. Effect of brine salinity on the
502 geological sequestration of CO₂ in a deep saline carbonate formation. Greenhouse Gases: Science
503 and Technology. 10(2), 296-312. doi:10.1002/ghg.1960.

504 Lamert, H., Geistlinger, H., Werban, U., Schutze, C., Peter, A., Hornbruch, G., Schulz, A., Pohlert, M.,
505 Kalia, S., Beyer, M., Grobmann, J., Dahmke, A., Dietrich, P., 2012. Feasibility of geoelectrical
506 monitoring and multiphase modeling for process understanding of gaseous CO₂ injection into a
507 shallow aquifer. Environmental Earth Sciences, 67(2), pp.447–462.

508 Little, M.G., Jackson, R.B., 2010. Potential Impacts of Leakage from Deep CO₂ Geosequestration on
509 Overlying Freshwater Aquifers, Environ. Sci. Technol. 44 (23), 9225–9232. DOI: 10.1021/es102235w.

510 Metz, B., Davidson, O., Coninck, H., Loos, M., Meyer, L., 2005. IPCC special report on carbon dioxide
511 capture and storage, Intergovernmental Panel on Climate Change, Geneva (Switzerland). Working
512 Group III. Cambridge University Press. [https://www.ipcc.ch/pdf/special-](https://www.ipcc.ch/pdf/special-reports/srccs/srccs_wholereport.pdf)
513 [reports/srccs/srccs_wholereport.pdf](https://www.ipcc.ch/pdf/special-reports/srccs/srccs_wholereport.pdf) [Accessed 31 October 2017].

514 Myer, L., 2011. Global Status of Geologic CO₂ Storage Technology Development, A report from the
515 U.S. Carbon Sequestration Council, [http://www.iea-coal.org.uk/documents/82579/7892/Global-status-](http://www.iea-coal.org.uk/documents/82579/7892/Global-status-of-geologic-CO2-storage-technology-development)
516 [of-geologic-CO2-storage-technology-development](http://www.iea-coal.org.uk/documents/82579/7892/Global-status-of-geologic-CO2-storage-technology-development) [Accessed 02 November 2016].

517 Petit, A., Cerepi, A., Loisy, C., Le Roux, O., Rossi, L., Chiquet, P., Estublier, A., Gance, J., Garcia, B.,
518 Gauchet, L., Hautefeuille, B., Lavielle, B., Van Lang, L., Noirez, S., Texier, B., Bachaud, P., Bouquet,
519 S., 2020. Aquifer-CO₂ Leak project: Physicochemical characterization of the CO₂ leakage impact on a
520 carbonate shallow freshwater aquifer, EGU General Assembly 2020, doi: 10.5194/egusphere-
521 egu2020-13889.

522 Petrik, C., Mabee, S.B., 2011. Experimental summarizing the potential of CO₂ sequestration in the
523 basalts of Massachusetts-Final report prepared for Massachusetts Clean Energy
524 Center, Boston. [http://www.geo.umass.edu/stategeologist/Products/reports/BasaltSequestrationReport.](http://www.geo.umass.edu/stategeologist/Products/reports/BasaltSequestrationReport.pdf)
525 pdf. [Accessed 25 July 2016].

526 Rabiou, K.O., Han, L., Das, D.B., 2017a. CO₂ Trapping in the Context of Geological Carbon
527 Sequestration, In: Abraham, M.A. (Ed.), *Encyclopedia of Sustainable Technologies*. Elsevier, pp. 461-
528 475, DOI:10.1016/B978-0-12-409548-9.10124-1.

529
530 Rabiou, K.O., Abidoye, L.K., Das, D.B., 2017b. Geo-Electrical Characterisation for
531 CO₂ Sequestration in Porous Media. *Environ. Process*, 4(2), pp. 303-317, doi:10.1007/S40710-
532 017-0222-2.

533 Snaebjornsdottir, S.O., Sigfusson, B., Marieni, C., Goldberg, D., Gislason, S.R., Oelkers, E.H., 2020.
534 Carbon dioxide storage through mineral carbonation, *Nature reviews, Earth and Environment*, 1, pp.
535 90-102, doi:10.1038/s43017-019-0011-8.

536 Song, Y., Sung, W., Jang, Y., Jung, W., 2020. Application of an artificial neural network in predicting
537 the effectiveness of trapping mechanisms on CO₂ sequestration in saline aquifers, *International*
538 *Journal of Greenhouse Gas Control*, 98, doi: 10.1016/j.ijggc.2020.103042.

539 Suekane, T., Furukawa, N., Tsushima, S., Hirai, S., Kiyota, M., 2009. Application of MRI in the
540 Measurement of Two-Phase Flow of Supercritical CO₂ and Water in Porous Rocks. *Journal of Porous*
541 *Media*, 12 (2), pp. 143-154, DOI: 10.1615/JPorMedia.v12.i2.40.

542 Szulczewski, M.L., 2013. The Subsurface Fluid Mechanics of Geologic Carbon Dioxide Storage. (PhD
543 Thesis) Massachusetts Institute of Technology, USA.
544 https://sequestration.mit.edu/pdf/2013_MikeSzulczewski_MIT-PhD_thesis.pdf [Accessed 25 July
545 2019].

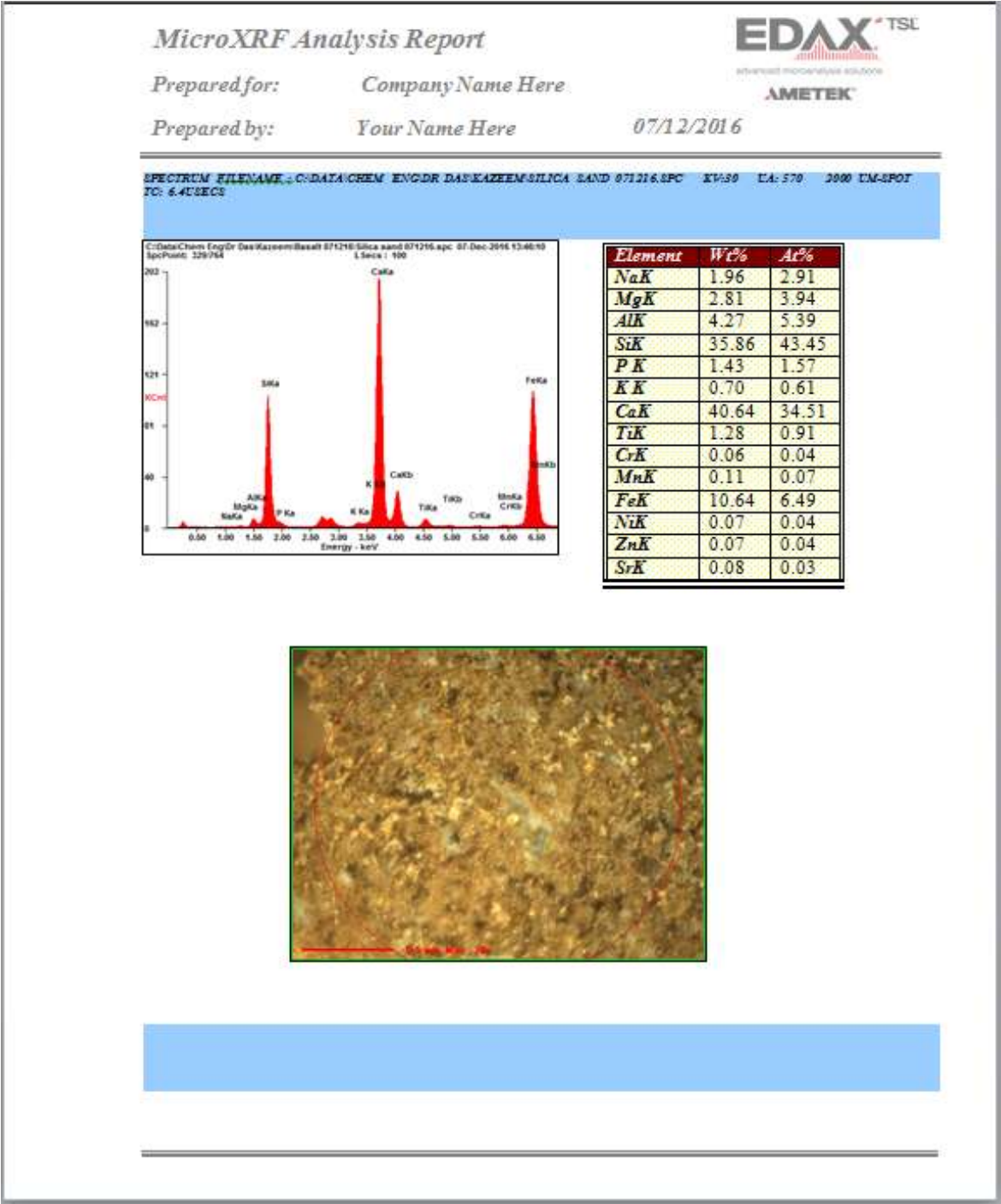
546 Talapatra, A. A., 2020. Study on the carbon dioxide injection into coal seam aiming at enhancing coal
547 bed methane (ECBM) recovery. *J Petrol Explor Prod Technol*, 10, pp. 1965–1981.
548 <https://doi.org/10.1007/s13202-020-00847-y>.

549 Terzi, K., Aggelopoulos, C.A., Bountas, I., Tsakiroglou, C.D., 2014. Effects of carbon dioxide on the
550 mobilization of metals from aquifers. *Environ. Sci. Technol*, 48, pp. 4386–4394.
551 http://www.peacesoftware.de/einigewerte/co2_e.html [Accessed 23 September 2016].

552 Wan, L., Han, M., Aljanobi, H., Zhdanov, M. 2018. Feasibility study of gravity gradiometry monitoring
553 of CO₂ sequestration in deep reservoirs using surface and borehole data, SEG Technical Program
554 Expanded Abstract, doi: 10.1190/segam2018-2996382.1.

555 White, S., Carroll, S., Chu, S., Bacon, D., Pawar, R., Cumming, L., Hawkins, J., Kelley, M.,
556 Demirkanli, I., Middleton, R., Sminchak, J., Pasumarti, A (2020). A risk-based approach to evaluating
557 the Area of Review and leakage risks at CO₂ storage sites. *International Journal of Greenhouse Gas*
558 *Control*, 93, art. no. 102884. DOI: 10.1016/j.ijggc.2019.102884.

559 Yang, X., Buscheck, T.A., Mansoor, K., Wang, Z., Gao, K., Huang, L., Appriou, D., Carroll, S.A.
560 (2019). Assessment of geophysical monitoring methods for detection of brine and CO₂ leakage in
561 drinking water aquifers. *International Journal of Greenhouse Gas Control*, 90, art. no. 102803,
562 DOI: 10.1016/j.ijggc.2019.102803.



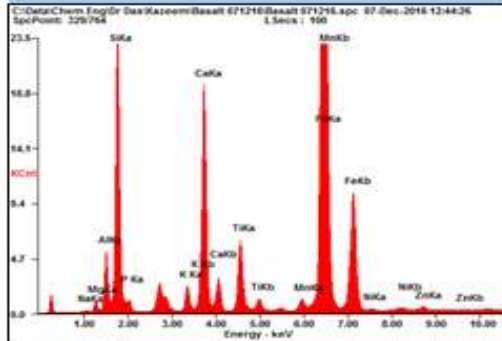
MicroXRF Analysis Report

Prepared for: Company Name Here

Prepared by: Your Name Here

07/12/2016

SPECTRUM FILENAME : C:\DATA\CHEM\ENQDR DAS KAZEM\BASALT 071216\BASALT 071216.SPC KV:50 UA:500 2000
UN-SPOT TO: 6.4USECS



Element	Wt%	At%
NaK	4.96	6.78
MgK	9.28	12.01
AlK	12.00	13.99
SiK	38.15	42.71
PK	2.03	2.06
KK	1.78	1.43
CaK	12.85	10.08
TiK	2.83	1.86
MnK	0.27	0.15
FeK	15.76	8.87
NiK	0.03	0.02
ZnK	0.07	0.04

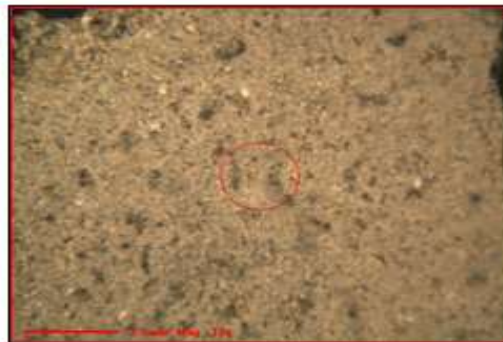


Figure A2 X-Ray Fluorescence (XRF) mineral analysis for Basalt sand particles.